NANO LETTERS

2004
Vol. 4, No. 5
805−810

How to Identify Haeckelite Structures: A Theoretical Study of Their Electronic and Vibrational Properties

X. Rocquefelte,[†] G.-M. Rignanese,[†,‡] V. Meunier,[§] H. Terrones,[||] M. Terrones,[||] and J.-C. Charlier*,[†,‡]

Unité de Physico-Chimie et de Physique des Matériaux (PCPM), Université Catholique de Louvain, Place Croix du Sud 1, B-1348 Louvain-La-Neuve, Belgium, Research Center on Microscopic and Nanoscopic Electronic Devices and Materials (CERMIN), Université Catholique de Louvain, B-1348 Louvain-La−Neuve, Belgium, Computer Science and Mathematics Division, Oak Ridge National Laboratory, Oak Ridge, Tennessee 37831, and Advanced Materials Department, IPICYT, Av. Venustiano Carranza 2425-A, San Luis Potosí 78210, México

Received January 20, 2004; Revised Manuscript Received March 9, 2004

ABSTRACT

First-principles (FP) calculations of the electronic and vibrational properties of three different Haeckelite structures have been performed. The relatively low cohesive energies (when compared to C_{60}) of these phases suggest the possible synthesis of such novel carbon arrangements. In agreement with previous tight-binding calculations (Terrones, H.; Terrones, M.; Hernandèz, E.; Grobert, N.; Charlier, J.-C.; Ajayan, P. M. *Phys. Rev. Lett.* 2000, *84*, 1716), the Haeckelite structures exhibit a clear metallic behavior. In addition, within the ab initio framework, we predict the IR and Raman frequencies, which constitute the fingerprint of their structure and allow for their unambiguous identification. STM images and quantum conductances of various tubular Haeckelite structures are also calculated within a tight-binding framework. The three investigated Haeckelite structures are shown to be good candidates of conducting wires with great potential in nanoelectronics. The results presented here provide a catalog of properties that will aid in the identification of other Haeckelite structures as well as carbon systems containing pentagonal and heptagonal defects.

Following their identification by Iijima in 1991,[2] carbon nanotubes (CNTs) have attracted considerable attention for their fascinating electronic and mechanical properties. Specifically, it has been theoretically predicted and experimentally demonstrated that CNTs could exhibit electronic properties ranging from small gap semiconductors to good conductors.[3,4]

Because of their quasi one-dimensional electronic structure, electronic transport in metallic CNTs occurs ballistically (i.e., without scattering).[5] However, various effects at the nanoscale could perturb such ideal situation: (i) the hybridization of the σ^* and π^* states of the graphene network[6] due to tube curvature, and (ii) the presence of topological defects.[7] In the latter case, it has been demonstrated that the creation of bond rotation defect (the so-called "Stone−Wales" defect) closes the gap in large-gap CNTs, opens the gap in small-gap CNTs, and increases the density of states at the Fermi level in metallic CNTs.[7] This behavior can be understood by analyzing a graphene sheet, in which pentagon−heptagon defects perturb the sp^2 carbon framework. As a direct consequence, the band dispersion at the Fermi level ($\pi-\pi^*$ states) and the Fermi surface are drastically modified.

Crespi et al.[8] proposed an alternative theoretical way to generate metallic carbon sheets by considering an ordered planar arrangement consisting only of pentagons and heptagons. As opposed to a graphene layer, which is a semimetal, the planar structure proposed by Crespi and coworkers exhibits a finite density of states at the Fermi level and could be considered as a good metal. This indicates that pentagon−heptagon defects induce a dramatic increase of the metallicity within CNTs.

By extrapolating this idea, a new family of metallic layered sp^2-like carbon crystals was proposed.[1] These novel systems, now termed Haeckelites, are characterized by the presence of a large number of pentagons and heptagons, in addition to the hexagons, which typically cover a graphitic plane. Their stability and unique electronic and mechanical properties were predicted within a tight-binding (TB) framework.[1] From the electronic point of view, the new family of carbon-based structures is characterized by remarkably high densities

* Corresponding author.
[†] Unité de Physico-Chimie et de Physique des Matériaux (PCPM), Université Catholique de Louvain.
[‡] CERMIN, Université Catholique de Louvain.
[§] Oak Ridge National Laboratory.
[||] IPICYT.

10.1021/nl049879x CCC: $27.50
Published on Web 04/07/2004

of states at the Fermi level, an effect caused by the presence of the large number of odd-membered rings within the structure.

An analysis based on the structural stability of Haeckelites, compared to graphite and C_{60} molecule, suggests that they could be synthesized in the laboratory. However, no experimental evidence of their existence has been reported hitherto. It is therefore important to predict and characterize their physical properties that will ultimately allow for researchers their experimental identification.

This account focuses on the properties of three different Haeckelite structures. First-principles calculations are used to confirm their stability and to investigate their electronic properties and vibrational spectra. The latter allows for the unambiguous identification of different phases using Raman scattering or IR absorption techniques. Finally, semiempirical tight-binding is used to compute the scanning tunneling microscopy (STM) images and quantum conductance properties of one-dimensional tubular Haeckelite structures obtained from the planar phases. STM is a technique that permits the clear identification of the atomic configuration on a surface. Although STM does not actually provide a direct information on the atomic arrangement *per se*, it probes the electronic density around the Fermi energy and is remarkably sensitive to highly localized states. The goal of this paper is to set up a catalog of physico-chemical properties that will help researchers in the identification of such highly defective systems, and subsequently to the exploitation of their remarkable properties.

The atomic coordinates and the cell parameters of all the structures are fully relaxed within density functional theory, as implemented in the ABINIT package.[10] The exchange-correlation energy is evaluated using the generalized gradient approximation of Perdew−Burke−Ernzerhof.[9] Only valence electrons are explicitly considered, and norm-conserving nonlocal pseudopotentials are used to account for the core−valence interactions.[11] The wavefunctions are expanded in plane waves up to a kinetic energy cutoff of 30 Ha, and the *k*-point sampling for the various phases is chosen sufficiently fine to ensure the numerical convergence of all the calculated properties.

The dynamical properties such as phonon frequencies at the zone center are conventionally computed as second-order derivatives of the total energy with respect to atomic displacements. The latter are obtained using a variational approach to density-functional perturbation theory, also implemented in the ABINIT package.

STM images have been computed using a well-tested semiempirical approach that is applied routinely in the identification of carbon nanotubes. It is based on the Tersoff−Hamman formalism for the tunneling current between a metallic tip and a substrate, as outlined in ref 12.

We first study the stability of three planar Haeckelite structures and compare our results to the stability of a pristine graphene sheet. The graphitic plane can be considered as a collection of hexagonal motifs (Figure 1a). However, Haeckelite structures in turn consist of an equal number of pentagons and heptagons, in addition to a number of hexagons (Figure 1b−d). The hexagonal carbon patterns are drawn in thick lines in Figure 1 in order to highlight the differences between the various models. Since the three Haeckelite crystals have different symmetry, we will adopt the following designation: $R_{5,7}$, $O_{5,6,7}$, $H_{5,6,7}$ for the rectangular, the oblique, and the hexagonal Haeckelite models, respectively. The subscripts refer to the type of polygons presents in the unit cell. For example, the rectangular model ($R_{5,7}$) does not contain any hexagon. In its unit cell, the heptagons and pentagons are paired symmetrically on a flat surface (Figure 1b), and was originally proposed by Crespi et al. [8] It can be visualized as the result of successive application of Stone−Wales (SW) rotations of a graphene plane (a SW rotation consists in the transformation of pyrene-like ring into two pairs of heptagons and pentagons). The primitive cell for the oblique model ($O_{5,6,7}$) is composed of pentalene and heptalene units bound together and surrounded by six-membered rings (Figure 1c). The hexagonal structure ($H_{5,6,7}$) exhibits repetitive units of three agglomerated heptagons, surrounded by alternating pentagons and hexagons (Figure 1d).

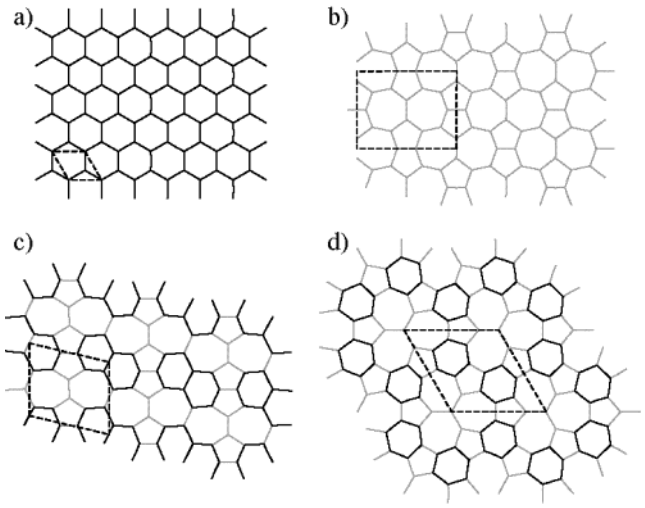

Figure 1. Schematic representation of four different layered sp^2-like carbon atomic arrangements with their respective unit cell: (a) graphite, (b) rectangular ($R_{5,7}$), (c) oblique ($O_{5,6,7}$), (d) hexagonal ($H_{5,6,7}$). The six-membered rings are highlighted.

The supercell method is used to perform the structural relaxations. In this scheme, the thickness of the unit cell (i.e., in the direction perpendicular to the plane) was chosen sufficiently large in order to avoid any spurious image effects on the calculated total energy and vibrational frequencies. In Table 1, we report the space group and the relative energy per atom with respect to graphene for C_{60} and the three Haeckelite structures, respectively. For comparison, the energy values obtained from TB calculations[1] are also listed in this table. Although FP and TB values are significantly different, both methods show comparable trends in the relative stability of the three Haeckelite phases: $E(H_{5,6,7}) < E(R_{5,7}) < E(O_{5,6,7})$. We found that the three relaxed structures turn out to be metastable when compared to the graphene sheet, while they are significantly more stable than C_{60}, a result which is in qualitative agreement with previous TB

Table 1. Symmetry and Relative Stability of Haeckelite Planar Structures with Respect to Graphene (meV/atom)

	point or space group	TB	FP
C_{60}	I_h	419	380
$O_{5,6,7}$	$P2/m$	408	375
$R_{5,7}$	$Cmmm$	307	261
$H_{5,6,7}$	$P6_2m$	304	246
graphene	$P6_3/mmc$	0	0

calculations. We also note that the most stable Haeckelite structure, $H_{5,6,7}$ (246 meV/atom), has no pentagon−pentagon adjacency, whereas the two other phases, $R_{5,7}$ (261 meV/atom) and $O_{5,6,7}$ (375 meV/atom), display a single pentagon−pentagon contact per unit cell. Therefore, TB and FP results suggest that Haeckelite arrangements also follow the "isolated pentagon rule" (IPR),[13] a phenomenological rule generally accepted in the context of fullerene structures.

The band structures and the total densities of states (DOS) for graphene and the rectangular, oblique, and hexagonal Haeckelite phases are given in Figures 2a, 2b, 2c, and 2d, respectively. The Fermi level is identified by a dotted line and is taken as the energy of reference. The graphene DOS exhibits the step function typical to two-dimensional layered structures. At first glance, the reason for the presence of such a shape in the three Haeckelite models is not obvious, although the DOS is oscillating with marked features around a constant value. This behavior can be attributed to bands that are less disperse (i.e., sharper peaks in the DOS) in Haeckelite phases than in graphite (see band structures in Figure 2). This is a direct consequence of the band folding, which is due to two main factors: a larger size of the primitive unit cell (4 atoms for graphite; 8 for $R_{5,7}$; 12 for $O_{5,6,7}$; 16 for $H_{5,6,7}$) and the loss of symmetry. Another important modification takes place when going from graphene to Haeckelite systems. A non-zero density of states is observed at the Fermi level, confirming the metallicity of the three Haeckelite crystals. This observation confirms previous TB calculations, for which only π electrons were taken into account (one-electron picture). For the hexagonal Haeckelite phase, the DOS exhibits a particularly intense peak at the Fermi level (see Figure 2d), characteristic of these types of systems.

The calculated phonon frequencies and their symmetry assignments for graphene and Haeckelite structures are summarized in Tables 2−5. The calculated IR absorption spectra and the Raman peak positions are presented in Figure 3. As no experimental information on the Haeckelite planar structures is available yet, we start by discussing the calculated vibrational frequencies of graphene, for which experimental values are available.[14] An excellent agreement between the theoretical and experimental values is presented in Table 2. This indicates that the theoretical method used is appropriate for predicting the vibrational modes of other forms of sp^2 carbon structures such as Haeckelite arrangements.

From the experimental point of view, IR and Raman spectroscopic techniques will provide characteristic features

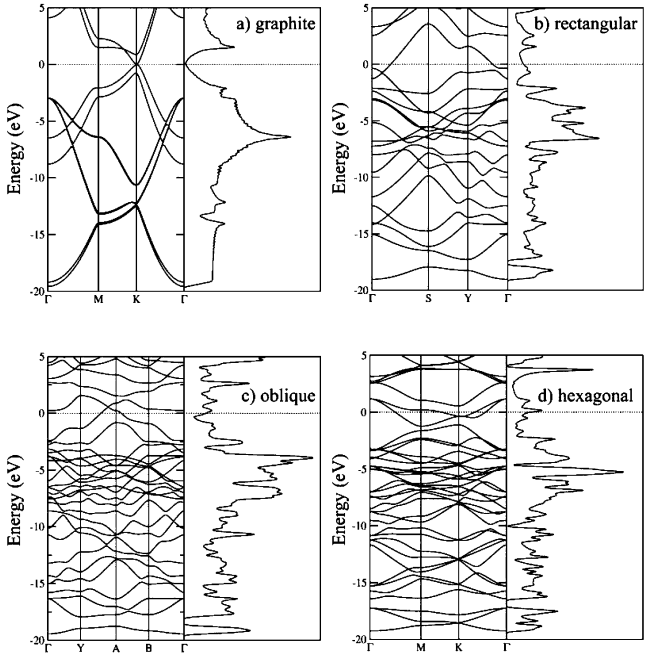

Figure 2. Band structure and electronic density of states (Fermi level positioned at zero energy) for graphite exhibiting semimetallic behavior (a) and for Haeckelites (b), (c), (d) showing metallic behavior. (b) rectangular ($R_{5,7}$), (c) oblique ($O_{5,6,7}$), (d) hexagonal ($H_{5,6,7}$). In all plots, the units of the density of states are states per eV.

Table 2. Calculated and Experimental Phonon Frequencies of Graphite (in cm^{-1}) with Their Symmetry Assignments

D_{6h} (6/mmm)	this work	expt.
Raman		
E_{2g} (1)	46.9	42
E_{2g} (2)	1592.6	1582
Infrared		
A_{2u} (1)	886.2	868
E_{1u} (2)	1601.8	1587
Silent		
B_{1g} (1)	127.3	127
B_{1g} (2)	880.2	-

for different types of defects (e.g., non hexagonal) within sp^2-hybridized carbons. As shown in Figure 3, the simulated IR spectra for different planar Haeckelites exhibit very different features from one phase to another. For graphene, it is worth noting that among the two allowed IR peaks only one (at 1602 cm^{-1}) gives rise to an intense signal (Figure 3a). Similar behavior is observed for the Haeckelite structures (Figures 3b−3d); only few symmetry allowed peaks lead to intense response in the IR mode. Two intense signals (at 1173 and 1279 cm^{-1}) are especially unique to the rectangular arrangement, whereas three (at 1440, 1547, and 1677 cm^{-1}) and one (at 1254 cm^{-1}) are obtained for oblique and hexagonal phases, respectively. Furthermore, these differences also occur among the different Haeckelites in the Raman vibrational frequencies, leading to the observation that both Raman scattering and IR absorption spectroscopy are well-suited experimental techniques for the identification of Haeckelite structures.

Table 3. Calculated Phonon Frequencies of $H_{5,6,7}$ (in cm^{-1}) with Their Symmetry Assignments

D_{3h} (62m)					
Raman					
E″	222.1	312.9	530.0	677.2	760.3
A_1'	561.0	1019.3	1349.0	1517.8	1714.6
Infrared					
A_2''	369.9	699.6	813.9		
IR + Raman					
E′	532.4	674.0	918.6	1001.9	1227.6
	1253.8	1282.8	1446.8	1615.2	1643.2
Silent					
A_1''	169.8	824.0			
A_2'	702.8	906.3	1039.7	1242.2	1491.1

Table 4. Calculated Phonon Frequencies of $R_{5,7}$ (in cm^{-1}) with Their Symmetry Assignments

D_{2h} (*mmm*)				
Raman				
B_{3g}	447.2	795.7		
B_{2g}	461.9	783.7		
B_{1g}	815.0	1022.0	1420.2	1586.2
A_g	1145.8	1452.5	1488.1	1606.9
Infrared				
B_{1u}	397.3	650.6		
B_{3u}	555.3	1172.7	1279.0	
B_{2u}	830.6	1098.5	1594.2	
Silent				
A_u	438.7			

Table 5. Calculated Phonon Frequencies of $O_{5,6,7}$ (in cm^{-1}) with Their Symmetry Assignments

C_{2h} (*mmm*)					
Raman					
B_g	234.7	270.5	584.9	714.0	770.5
	825.0				
A_g	617.3	756.7	841.1	1036.4	1064.5
	1145.0	1215.6	1432.8	1443.8	1557.8
	1697.5	1767.7			
Infrared					
A_u	209.4	350.1	459.6	667.0	736.2
B_u	505.0	643.4	806.3	946.8	1048.8
	1163.7	1321.1	1440.2	1547.0	1677.4

The vibrational analysis of Haeckelite structures is a sensitive issue, since non-hexagonal rings are sharing edges in such topologies. In the present study, the structures involved include pentagon−pentagon pairs and pentagon−heptagon pairs, which means that neither heptagons nor pentagons are completely isolated in the hexagonal network (as pentagons would be in C_{60}, for example). Consequently, the attribution of IR or Raman active modes to pentagonal or heptagonal rings is not straightforward. However, in the three structures investigated here, three active Raman modes (R: 1453 cm^{-1} ; O: 1433 cm^{-1} ; H: 1447 cm^{-1}) are mainly localized on the pentagons. These modes are in the same range of frequencies as for the pentagonal mode of the corannulene molecule ($A_1(7)$ = 1414 cm^{-1}) and the pentagonal pinch mode of the C_{60} ($A_g(2)$: 1470 cm^{-1}) and display an analogous pattern for the atomic displacements.

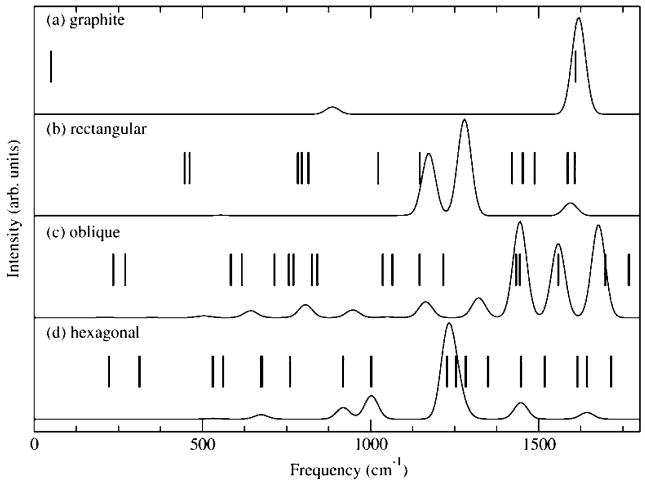

Figure 3. Simulated infrared absorption spectra for graphite (a) and Haeckelite planar structures (b), (c), (d): (b) rectangular ($R_{5,7}$), (c) oblique ($O_{5,6,7}$), (d) hexagonal ($H_{5,6,7}$). The Raman frequencies (vertical lines) are also given.

Similar to carbon nanotubes, Haeckelite sheets can be rolled up in such a way as to form hollow cylinders. In this study, we also considered three Haeckelite nanotubes obtained by rolling up the three flat systems considered above. We have computed their STM images for positive (+0.4 V) and negative (−0.4 V) tip−substrate bias potential. The potential is applied in such a way that occupied states of the tubes are imaged for positive bias while unoccupied states determine the image obtained with negatively polarized tip. The simulated STM images are reproduced on Figure 4. We remark that the superimposed atomic structure is barely recognizable from the simulated images, and those images computed for opposite tip polarities are unmistakably different. These two characteristics are explained by the fact that the tunneling current mainly originates from nanotube-centered localized donor (positive bias) and acceptor (negative bias) states, corresponding to the high density of heptagons and pentagons, respectively. This result shows that the identification of tubular Haeckelite structures is a challenging task using topographic techniques, even more when no simulation or modeling is available. Incidentally, it is possible that these structures have been already observed but were inadvertently missed, since even high spatial resolution STM images do not directly reveal the underlying atomic structure.

The proposition of new carbon allotropes with a large number of pentagons and heptagons was originally motivated by the search for better metallic compounds, i.e., systems with an increased DOS at the Fermi level and a higher electronic conductivity. In order to check the validity of the systems proposed here, we need to investigate their electronic transport properties. We investigated the transport properties within the Landauer formalism using a Green's function and transfer-matrix-based approach for computing electron transport in extended systems.[15] Note that the results reported in

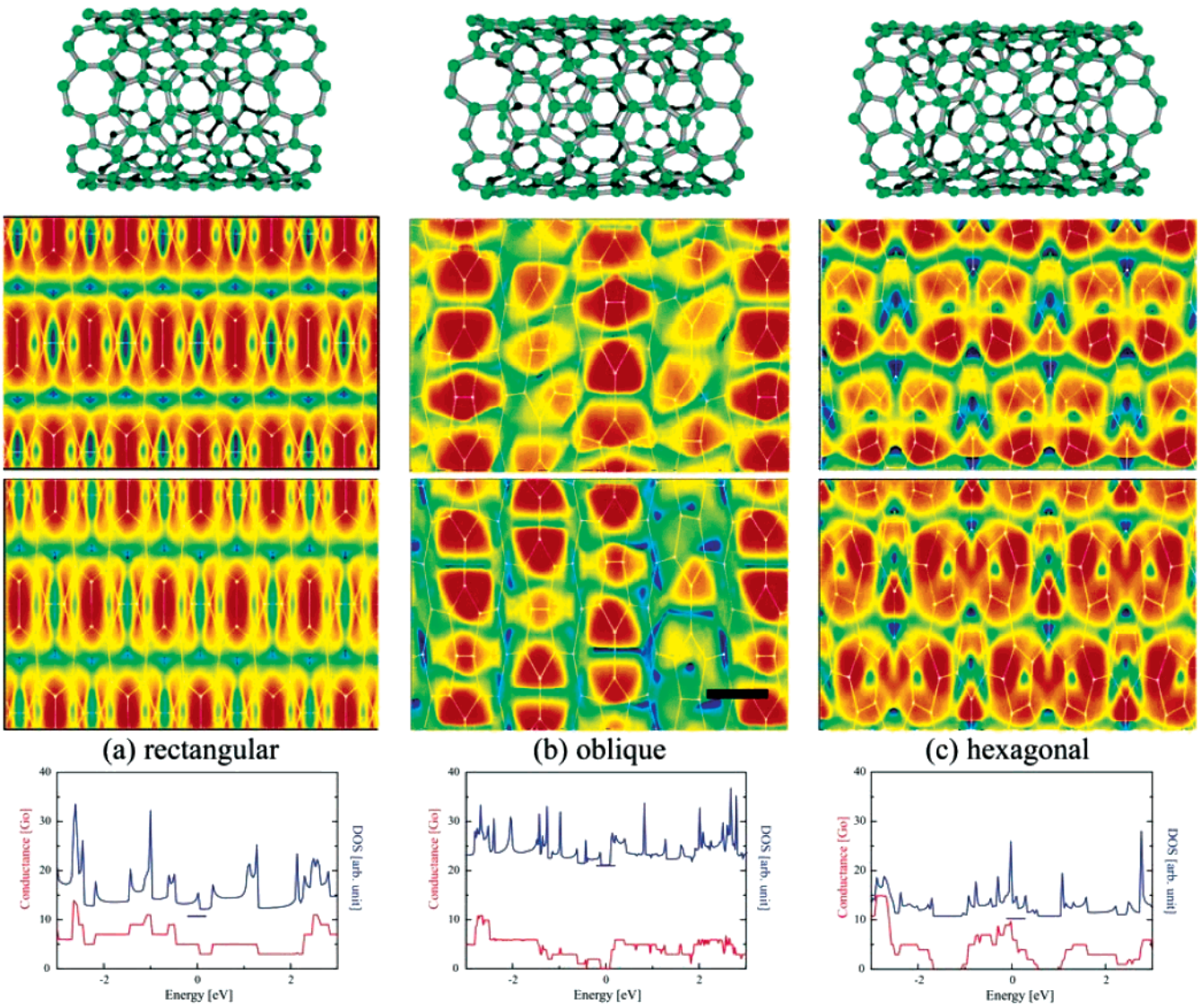

Figure 4. STM image simulation (top) and electronic conductance (bottom) for the tubular Haeckelite structures (a) rectangular ($R_{5,7}$), (b) oblique ($O_{5,6,7}$), (c) hexagonal ($H_{5,6,7}$). The black solid line bar in the central STM image represents a length of 5 Å.

Figure 4 are bulk-like calculations, which means that they were obtained by seamlessly connecting the central "conductor" to electron reservoirs on the left and on the right by leads made up of the same structure. The conductance spectra are derived from the electronic band dispersion, and the number of channels is merely a counting of the bands for a given energy. Figure 4 depicts the electron conductance of Haeckelite structures. For example, the rectangular-based and hexagonal-based Haeckelite tubules exhibit a large number of available conducting channels at the Fermi level, whereas the oblique displays a small gap around the Fermi level. Although our study demonstrates that Haeckelite structures display an intrinsic metallic transport when compared to hexagonal carbon nanotubes of similar radii, our study does not assess the robustness of the conducting channels, in other words, how these channels couple with metallic leads in a practical transport experiment. This is important information, but a full investigation with realistic leads goes beyond the scope of this study.

In summary, we have calculated the structural and the vibrational properties of three different Haeckelite arrangements using first-principles calculations. Haeckelites are found to be metastable with respect to a pure graphene sheet, and more stable than C_{60} as already predicted by semi-empirical methods. In addition, Haeckelite tubes exhibit an improved metallic character when compared to the zero-gap semiconducting graphene sheet. Finally, various ways of characterization are proposed. In particular, infrared and Raman studies allow us to distinguish different carbon structures unambiguously. The present results could also be used in order to identify haeckelite-type topological defects. This could be particularly promising in the understanding of the atomic structure of coiled carbon nanotubes. Using STM experiments, Biro et al. have highlighted the tubular structure of these carbon systems.[16,17] In order to explain the helicoidal character of the phases, these authors proposed a regular organization of non-hexagonal rings in order to produce haeckelite-type structures.[18] Haeckelite crystals have

not been identified experimentally, but the IR, Raman, and STM simulated data presented in this account will provide experimentalists with additional evidence for detecting such fascinating carbon allotropes.

Acknowledgment. G.M.R. and J.C.C. acknowledge the National Fund for Scientific Research [FNRS] of Belgium for financial support. This paper presents research results of the Belgian Program on Inter-university Attraction Poles (PAI5/1/1) entitled *Quantum Size Effects in Nanostructured Materials* and of the Action de Recherche Concertée entitled *Interaction électron-phonon dans les nanostructures*, sponsorded by the Communauté Française de Belgique. This work is carried out within the framework of the EU Human Potential − Research Training Network COMELCAN project (No. HPRN-CT-2000-00128). This research is also sponsored in part by the Mathematical Information and Computational Sciences Division, Office of Advanced Scientific Computing Research of the U.S. Departement of Energy under Contract No. DE-AC0500OR22725 with UT-Battelle, LLC. We also thank CONACYT-México grants: W-8001-millennium initiative (H.T., M.T.), G-25851-E (H.T., M.T.), 36365-E (H.T.), and 37589-U (M.T.) for financial support.

References

(1) Terrones, H.; Terrones, M.; Hernandèz, E.; Grobert, N.; Charlier, J.-C.; Ajayan, P. M. *Phys. Rev. Lett.* **2000**, *84*, 1716.
(2) Iijima, S. *Nature* **1991**, *354*, 56.
(3) Hamada, N.; Sawada, S.; Oshiyama, A. *Phys. Rev. Lett.* **1992**, *68*, 1579.
(4) Saito, R.; Fujita, M.; Dresselhaus, G.; Dresselhaus, M. S. *Appl. Phys. Lett.* **1992**, *60*, 2204.
(5) Mintmire, J. W.; Dunlap, B. I.; White, C. T. *Phys. Rev. Lett.* **1992**, *68*, 631.
(6) Blase, X.; Benedict, L. X.; Shirley, E. L.; Louie, S. G. *Phys. Rev. Lett.* **1994**, *72*, 1878.
(7) Crespi, V. H.; Cohen, M. L.; Rubio, A. *Phys. Rev. Lett.* **1997**, *79*, 2093.
(8) Crespi, V. H.; Benedict, L. X.; Cohen, M. L.; Louie, S. G. *Phys. Rev. B* **1996**, *53*, R13303.
(9) Perdew, J. P.; Burke, K.; Ernzerhof, M. *Phys. Rev. Lett.* **1996**, *77*, 3865.
(10) Gonze, X.; Beuken, J. M.; Caracas, R.; Detraux, F.; Fuch, M.; Rignanese, G. M.; Sindic, L.; Verstraete, M.; Zerah, G.; Jollet, F.; Torrent, M.; Roy, A.; Mikami, M.; Ghosez, P.; Raty, J. Y.; Allan, D. C. *Comput. Mater. Sci.* **2002**, *25*, 478.
(11) Troullier, N.; Martins, J. L. *Phys. Rev. B* **1991**, *43*, 1993.
(12) Meunier, V.; Lambin, P. *Phys. Rev. Lett.* **1998**, *81*, 5588.
(13) Albertazzi, E.; Domene, C.; Fowler, P. W.; Heine, T.; Seifert, G.; Van Alsenoy, C.; Zerbetto, F. *Phys. Chem. Chem. Phys.* **1999**, *1*, 2913.
(14) Jishi, R. A.; Dresselhaus, G. *Phys. Rev. B* **1982**, *26*, 4514.
(15) Buongiorno Nardelli, M. *Phys. Rev. B* **1999**, *60*, 7828.
(16) Biro, L. P.; Mark, G. I.; Koos, A.; Nagy, J. B.; Lambin, P. *Phys. Rev. B* **2002**, *66*, 165405.
(17) Koos, A. A.; Ehlich, R.; Horvath, Z. E.; Osvath, Z.; Gyulai, J.; Nagy, J. B.; Biro, L. P. *Mater. Sci. Eng. C* **2003**, *23*, 275.
(18) Lambin, P.; Mark, G. I.; Biro, L. P. *Phys. Rev. B* **2003**, *67*, 205413.

NL049879X